Nitrogen-vacancy centers created by N$^+$ ion implantation through screening SiO$_2$ layers on diamond

Kazuki Ito, Hiroshi Saito, Kento Sasaki, Hideyuki Watanabe, Tokuyuki Teraji, Kohei M. Itoh, and Eisuke Abe

---

Articles you may be interested in

CrossMark
click for updates

Nitrogen-vacancy centers created by N$^+$ ion implantation through screening SiO$_2$ layers on diamond

Kazuki Ito,[1] Hiroshi Saito,[1] Kento Sasaki,[1] Hideyuki Watanabe,[2] Tokuyuki Teraji,[3] Kohei M. Itoh,[1,4,a)] and Eisuke Abe[4,b)]

[1]*School of Fundamental Science and Technology, Keio University, 3-14-1 Hiyoshi, Kohoku-ku, Yokohama 223-8522, Japan*
[2]*Correlated Electronics Group, Electronics and Photonics Research Institute, National Institute of Advanced Industrial Science and Technology (AIST), Tsukuba Central 5, 1-1-1 Higashi, Tsukuba, Ibaraki 305-8565, Japan*
[3]*National Institute for Materials Science, 1-1 Namiki, Tsukuba, Ibaraki 305-0044, Japan*
[4]*Spintronics Research Center, Keio University, 3-14-1 Hiyoshi, Kohoku-ku, Yokohama 223-8522, Japan*

We report on an ion implantation technique utilizing a screening mask made of SiO$_2$ to control both the depth profile and the dose. By appropriately selecting the thickness of the screening layer, this method fully suppresses the ion channeling, brings the location of the highest nitrogen-vacancy (NV) density to the surface, and effectively reduces the dose by more than three orders of magnitude. With a standard ion implantation system operating at the energy of 10 keV and the dose of 10^{11} cm^2 and without an additional etching process, we create single NV centers close to the surface with coherence times of a few tens of μs. *Published by AIP Publishing.*
[http://dx.doi.org/10.1063/1.4984060]

Impurity doping of semiconductors is a fabrication process indispensable for modern electronic devices and continues to be so for quantum devices such as silicon-based single-donor spin qubits,[1–3] in which the positions of the individual donors must be controlled precisely.[4] Being optically addressable and coherently controllable by microwaves, single electronic spins associated with the negatively charged nitrogen-vacancy (NV$^-$) centers in diamond play important roles in emergent quantum technology, e.g., as a matter qubit interfacing with a flying qubit[5–8] and as a nanoscale magnetic sensor.[9–11] Both applications demand that the NV centers should be located close to the diamond surface.[12] For quantum networks, shallow NV spins can be efficiently coupled to photons in a nanophotonic cavity.[13] For magnetometry, the proximity of the NV sensor to a magnetic specimen is crucial because their dipolar coupling strength decays as the inverse cube of the separation.

So far, shallow NV centers (< 5 nm from the surface) have been created primarily by (i) nitrogen-doping during CVD growth[14–17] and (ii) N$^+$ ion implantation.[18–27] The CVD approach allows the accurate control of the impurity distribution in the depth direction, whereas the doping is random in the lateral dimensions. Ironically, high-quality CVD diamond films tend to lack vacancies to pair up with nitrogen atoms; an additional process to introduce vacancies, such as electron irradiation,[14] C$^+$ ion implantation,[16] or He$^+$ ion implantation,[17] is often required although the creation of shallow NV centers in as-grown films has also been reported.[15]

Ion implantation introduces both nitrogen atoms and vacancies into diamond. The lateral distributions are controllable by the use of a focused ion beam[18] or an array of small apertures.[20–23] The main concern is that the depth profile intrinsically has broadening approximated by a Gaussian distribution. Importantly, the ions can penetrate deep inside the crystal lattice due to the ion channeling effect.[28] The prevailing approach is to keep the implantation energy low (< 5 keV).[24–27] It is also preferred to set the implantation dose (fluence) low ($\sim 10^8$ cm^{-2}) so that single NV centers can be resolved optically. On the other hand, standard, multipurpose ion implantation systems operate at 10 keV or higher with the dose of 10^{11} cm^{-3} or higher, making this approach not widely available. Even with high-energy ion implantation, it is possible to plasma-etch the implanted diamond to bring the NV centers closer to the surface. But special care must be taken to prevent the etching itself from damaging the surface.[29,30]

In this paper, we report on an ion implantation technique utilizing a screening mask made of SiO$_2$ to control both the depth profile and the dose. With a standard ion implantation system operating at the energy of 10 keV and the dose of 10^{11} cm^2 and without additional surface-etching, we create single NV centers close to the surface. The use of a screening mask is quite common in the silicon industry[28] and yet has not been explored thoroughly in the context of NV centers. Previously, thin (< 10 nm) or thick (~ 100 nm) screening layers were employed to mitigate the ion channeling or fully suppress the ion transmission into diamond[20–23] but not to control the entire depth profile. We show here that the appropriate selection of the screening layer thickness has a qualitatively different consequence that is preferable to create shallow NV centers.

To illustrate our approach, we carry out Monte Carlo simulations of ion implantation using a software package SRIM.[31,32] Figure 1(a) shows the simulation results for diamond and SiO$_2$ with the N$^+$ energy of 10 keV and the dose of 10^{11} cm^{-2}. The incident angle is normal to the surface. Fitting the curves by Gaussian distribution functions, we

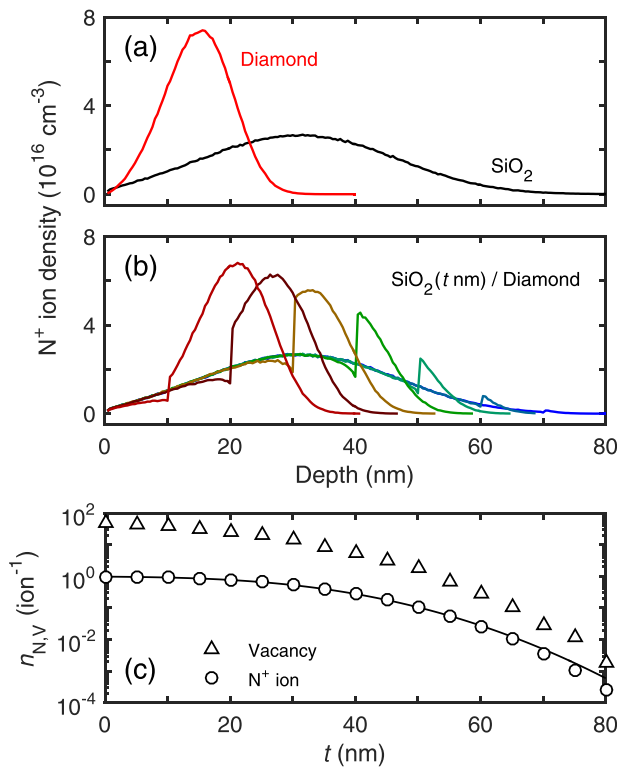a)Electronic mail: kitoh@appi.keio.ac.jp
b)Electronic mail: e-abe@keio.jp

FIG. 1. Monte Carlo simulations (SRIM) of (a) N^+ ion implantations into diamond and SiO_2 and (b) SiO_2 (t nm)/diamond heterostructures with $t = 10, 20, 30, 40, 50, 60,$ and 70 nm. The interfaces are discernible as vertical lines. (c) n_N ($\bigcirc$) and n_V ($\triangle$) as functions of t. The solid line is a calculation using Eq. (1).

obtain the *projected range* R (the mean travel distance of ions along the axis of the incidence) and the *projected straggle* σ (standard deviation) as $R_d = 15.0$ nm and $\sigma_d = 5.4$ nm for diamond, and $R_m = 31.1$ nm and $\sigma_m = 15.1$ nm for SiO_2, respectively. We note that SRIM does not take into account the ion channeling, and therefore, the actual depth profile for diamond can have a longer tail toward the interior of the material. On the other hand, SiO_2 is an amorphous material expected to be free of the ion channeling.

We then simulate the case of SiO_2 (t nm)/diamond heterostructures. Figure 1(b) shows the results for various t ranging between 10 and 70 nm with 10 nm steps. The depth profiles now appear as combinations of the profiles of the two materials; down to the SiO_2/diamond interfaces at t nm, the profiles trace that of SiO_2 (except for the small reductions near the interfaces), and after entering into diamond, the profiles mimic that of diamond with the near-surface parts truncated. Qualitatively, these profiles are analogous to the case in which N^+-ion-implanted diamond (without SiO_2) is surface-etched by $d_e = (\sigma_d/\sigma_m)(t - R_m) + R_d$ nm, where d_e is determined so that the integration of the profile for SiO_2 larger than t and that for diamond larger than d_e may be equal. Notably, for $t \geq 40$ nm ($> R_m$), only the tail parts appear in the profiles inside of diamond, and thereby, the locations of the highest ion densities are *at the surface*. It is also clear that the distributions in the depth direction become much narrower than σ_d. In addition, the simulated profiles should be more reliable for larger t, owing to the better suppression of ion channeling by SiO_2 layers.

In Fig. 1(c), we plot the fraction of N^+ ions transmitted into diamond n_N and the average number of vacancies in

diamond created by a single ion n_V. n_N (t) can also be estimated as[28]

$$n_N(t) = \frac{1}{2}\text{erfc}\left(\frac{t - R_m}{\sqrt{2}\sigma_m}\right), \qquad (1)$$

reproducing well the simulation results. Figure 1(c) shows that we are able to reduce the *effective* dose by three orders of magnitude, at the same time reducing the number of vacancies by nearly four orders of magnitude. The excess vacancies not diffused away or annihilated by thermal annealing after the ion implantation are the sources to degrade the crystalline quality; creating less vacancies at the stage of ion implantation can be beneficial. Assuming a moderate N-to-NV conversion efficiency (yield) of 1%, the final NV density of $\sim 10^{11}$ cm^{-3} (or $\sim 2 \times 10^7$ cm^{-2}), favorable to the single NV detection, is attainable.

The benefits of using a screening mask with an appropriately chosen thickness are summarized as follows: (i) the ion channeling is fully suppressed, (ii) the location of the highest NV density can be brought to the surface, and (iii) the effective dose can be reduced by more than three orders of magnitude.

We now test our approach experimentally. The sample was a natural abundant, (100)-oriented type-IIa high pressure high temperature (HPHT) diamond (Sumitomo), on which multiple SiO_2 layers with different thicknesses were deposited by electron beam evaporation. During the SiO_2 deposition and the N^+ ion implantation, the sample was kept covered with a metal plate equipped with apertures with the diameter of 400 μm. In each deposition run, only one aperture was open, and the rest of the apertures were blocked. On the sample stage of the evaporator, a silicon substrate was also set in the vicinity of the sample. After each run, we determined the thickness t of deposited SiO_2 by ellipsometry to the silicon substrate (the thickness of native oxide is taken into account). The sample was then implanted with $^{15}N^+$ ions at 10 keV and the dose $D_N = 10^{11}$ cm^{-2} (Ion Technology Center), with all the apertures open. The ^{15}N isotopes ($I = \frac{1}{2}$) were used to discriminate from the ^{14}N isotopes in the bulk ($I = 1$, 99.6%). After the ion implantation, the SiO_2 layers were removed by hydrofluoric acid. The sample was subsequently annealed at 800 °C for 2 h in vacuum in order to let vacancies diffuse to form NV centers, and at 450 °C for 9 h in an oxygen atmosphere in order to convert neutral NV (NV^0) centers into negatively charged ones (NV$^-$).[33] The sample was cleaned before and after each annealing process. In the following, the areas with $t = 0, 16, 25, 36, 46, 53, 64,$ and 72 nm are measured in detail.

The properties of the created NV centers are examined by fluorescence imaging and optically detected magnetic resonance (ODMR), using a home-built confocal microscope combined with microwave circuitry. The photons emitted from the NV centers (625–800 nm) are collected by a single-photon counting module, and our setup typically gives $\sim$25 kcps (kilo-counts per second) photons from a single NV center located close to a diamond surface, which is calibrated using a different diamond sample containing near-surface NV centers (similar to the one reported in Ref. 15). Figure 2 shows representative fluorescence images taken at different areas of the sample surface. As t increases, the photon counts
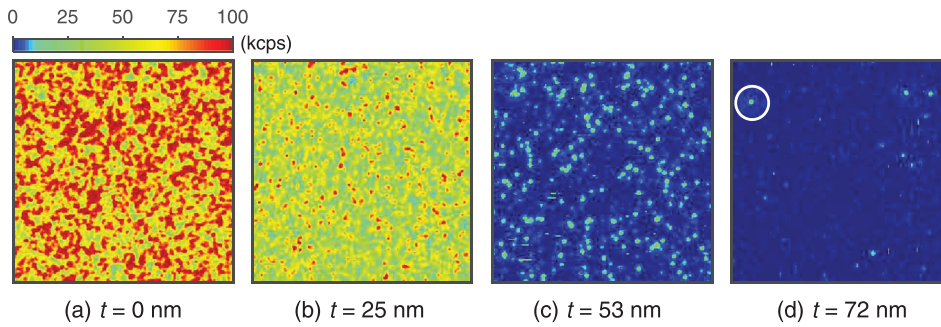
0   25   50   75   100
(kcps)

(a) $t = 0$ nm   (b) $t = 25$ nm   (c) $t = 53$ nm   (d) $t = 72$ nm

FIG. 2. Fluorescence images (20×20 μm^2) of areas N^+-ion-implanted through SiO_2 layers with $t = 0$ nm (a), 25 nm (b), 53 nm (c), and 72 nm (d). The white circle indicates the spot from which the data in Figs. 4(a)–4(c) were taken.

from the surface progressively decrease. For the areas with $t \leq 36$ nm, we observe ensemble NV centers. In the $t = 46$ nm area, both the single and ensemble NV centers are observed. For the areas with $t \geq 53$ nm, large portions of the images are dark, with discrete spots emitting a few tens kcps photons as expected for single NV centers. We note that, in claiming NV centers (single or ensemble) here, they are confirmed to originate from ^{15}NV centers (see Fig. 4). We also note that from photoluminescence (PL) spectroscopy, we have not detected signals unrelated to NV centers, for instance silicon-vacancy (SiV) centers. It is possible that our method introduces Si atoms into diamond due to a knock-on effect and subsequently produces SiV centers. However, as far as we checked, such SiV centers have not been found, and we conclude that the knock-on of Si atoms during the N^+ ion implantation is negligible here.

We estimate the NV density N_{NV} in two ways. For the areas with $t \leq 46$ nm, where ensemble NV centers are observed, we calculate the average photon counts per laser spot size and divide them by the calibrated photon counts from a single NV center (25 kcps). As the depth resolution of our confocal microscope is at most a micron, much larger than the expected depth profile, we calculate the average NV number in the unit area (in cm^{-2} unit). For the areas with $t \geq 53$ nm, we count the number of bright spots in the observed region. To correctly identify single NV^- centers and exclude the signals from NV^0 as well as other spurious emitters such as surface dusts, the threshold values for photon counts and the spot size are defined. The estimated N_{NV} is shown in Fig. 3(a). For comparison, the N density N_N

calculated as $D_N \times n_N$ is given. Also given is $0.01 \times N_N$, which roughly follows the N_{NV} data points, indicating the yield of about 1%. Figure 3(b) plots the yield calculated as N_{NV}/N_N. It is observed that the yields for single NV centers are $\sim 0.2\%$, less efficient than those for ensemble NV centers ($\sim 3\%$). The better values in the ensemble case may partly be attributed to the inclusion of the phonon side band of NV^0 in the photon counts. Extending up to 700 nm, the phonon side band of NV^0 partially overlaps with the NV^- spectrum. However, from PL spectroscopy, we estimate the ratio $NV^-/$ $(NV^- + NV^0)$ to be around 80%; this is not sufficient to explain the difference in the yields. It is possible that the reduced number of vacancies for larger t [see Fig. 2(c)] resulted in the reduced probabilities of paring up a nitrogen atom and a vacancy. A further work is necessary to understand the t-dependence of the yield.

Next, we examine the spin properties of single NV centers found in the $t \geq 46$ nm areas. An example of the ODMR spectrum taken at the $t = 72$ nm area is shown in Fig. 4(a). The resonance dip corresponding to the $m_S = 0 \leftrightarrow -1$ transition is split by 14 MHz due to the hyperfine coupling with a proximal ^{13}C nucleus ($I = \frac{1}{2}$, 1%), attributed to the third shell.[34,35] The dips are further split by 3 MHz due to the hyperfine coupling with the ^{15}N nucleus of its own. Note that the $m_S = 0 \leftrightarrow 1$ resonances are 200 MHz higher and are not shown. In addition to giving ~ 25 kcps photons, the coupling to a specific ^{13}C nucleus in the lattice evidences that the observed spectrum arises from a single NV center. The ^{15}N hyperfine interaction unambiguously implies that the NV center is formed from the implanted nitrogen.

In measuring the coherence time T_2 of the NV spins by a Hahn-echo sequence,[36] two factors contributing the echo signal must be considered. One is the electron spin echo envelope modulation (ESEEM) effect due to the ^{15}N nucleus of the NV center,[14] and the other is the echo revivals due to ^{13}C nuclei in the bulk.[37] To mitigate them, we work at higher magnetic fields, as shown in Fig. 4(b). Aligned along the NV axis, the static magnetic field of a few tens of mT serves to polarize the ^{15}N nucleus and suppress the ^{15}N ESEEM. In addition, the revival period of the ^{13}C nuclear oscillation in this case is a few μs, thus cannot be overlooked even when T_2 is short. Figure 4(c) shows the echo decay curve obtained at the condition of (b), giving $T_2 = 9$ μs. We repeat the T_2 measurements for various single ^{15}NV centers, and the results for 40 NV centers are summarized in Fig. 4(d). One fourth of the measured NV centers have $T_2 > 10$ μs, and the longest T_2 we have obtained so far is 25.4 μs from the $t = 72$ nm area. On the other hand, a half of the measured NV

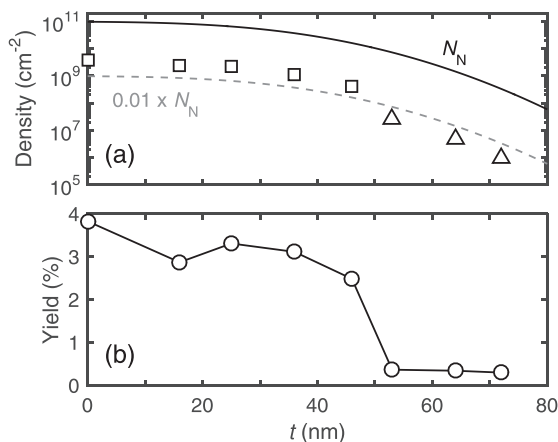
FIG. 3. (a) The experimental NV density N_{NV} and the calculated N density N_N, $0.01 \times N_N$, as functions of t. The square (triangle) points □ (△) are estimated from the ensemble (single) NV centers. (b) Yield (N_{NV}/N_N) as a function of t.
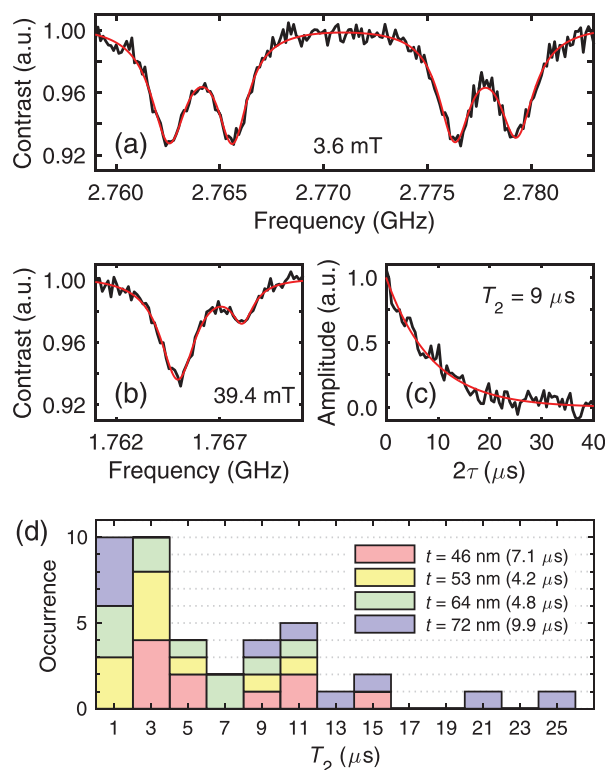
FIG. 4. (a) ODMR spectrum of a single NV center found at the $t = 72$ nm area [the white circle in Fig. 2(d)], exhibiting the hyperfine couplings with ^{13}C and ^{15}N nuclei. (b) ODMR spectrum of the same NV center as in (a) at higher magnetic fields. (c) Hahn echo decay curve taken at the condition of (b). (d) T_2 of single NV centers in areas N$^+$-ion-implanted through SiO$_2$ layers with $t = 46$, 53, 64, and 74 nm. For the respective areas, 10 NV centers are measured (the average T_2 times are given in the legend), and the results for 40 NV centers in total are shown as a stacked histogram. The bar width is 2 μs.

centers show short coherence with $T_2 < 4$ μs, hinting that they are very close to the surface. We leave a detailed study on the relationship between T_2 and the depth from the surface as a future work.

To summarize, we have proposed and demonstrated an ion implantation technique utilizing a screening mask made of SiO$_2$ to control both the depth profile and the dose. Even with the implantation energy of 10 keV and the dose of 10^{11} cm^2, which are in general too high to create shallow single NV centers, we are able to create single NV centers with T_2 of a few tens of μs. In addition to being simple and less demanding in the sense that neither a custom-built low-energy low-dose ion implantation system nor a careful plasma-etching process is required, this method is easily combined with the aperture array method to provide additional control in the lateral distribution. We also point out that a material for the screening mask is flexible and not limited to SiO$_2$; one can use other materials as long as their thicknesses are precisely controllable and they are preferably amorphous. AlO$_2$ or organic resists may be used, for instance. Future works include the determination of the depth profile of the NV centers by using, for instance, proton nuclear magnetic resonance (NMR) of external surface nuclear spins.[38] The present diamond substrate contains ^{13}C nuclei, the NMR signal of which can mimic that of protons.[39] The use of isotopically pure ^{12}C diamond as a starting material will avoid this problem and can also improve the

coherence properties of the NV spins. Relatively short T_2 observed here is indicative of the near-surface nature of the NV centers created, but it should also be noted that the nitrogen and vacancy distributions can be quite different from the standard ion implantation. To understand the formation dynamics of the NV centers both qualitatively and quantitatively, a combination of molecular dynamics and kinetic Monte Carlo simulations will be important.[40]

[1]B. E. Kane, Nature **393**, 133 (1998).
[2]J. J. Pla, K. Y. Tan, J. P. Dehollain, W. H. Lim, J. J. L. Morton, D. N. Jamieson, A. S. Dzurak, and A. Morello, Nature **489**, 541 (2012).
[3]J. T. Muhonen, J. P. Dehollain, A. Laucht, F. E. Hudson, R. Kalra, T. Sekiguchi, K. M. Itoh, D. N. Jamieson, J. C. McCallum, A. S. Dzurak, and A. Morello, Nat. Nanotechnol. **9**, 986 (2014).
[4]J. van Donkelaar, C. Yang, A. D. C. Alves, J. C. McCallum, C. Hougaard, B. C. Johnson, F. E. Hudson, A. S. Dzurak, A. Morello, D. Spemann, and D. N. Jamieson, J. Phys.: Condens. Matter **27**, 154204 (2015).
[5]E. Togan, Y. Chu, A. S. Trifonov, L. Jiang, J. Maze, L. Childress, M. V. G. Dutt, A. S. Sørensen, P. R. Hemmer, A. S. Zibrov, and M. D. Lukin, Nature **466**, 730 (2010).
[6]H. Bernien, B. Hensen, W. Pfaff, G. Koolstra, M. S. Blok, L. Robledo, T. H. Taminiau, M. Markham, D. J. Twitchen, L. Childress, and R. Hanson, Nature **497**, 86 (2013).
[7]W. Pfaff, B. J. Hensen, H. Bernien, S. B. van Dam, M. S. Blok, T. H. Taminiau, M. J. Tiggelman, R. N. Schouten, M. Markham, D. J. Twitchen, and R. Hanson, Science **345**, 532 (2014).
[8]B. Hensen, H. Bernien, A. E. Dréau, A. Reiserer, N. Kalb, M. S. Blok, J. Ruitenberg, R. F. L. Vermeulen, R. N. Schouten, C. Abellán, W. Amaya, V. Pruneri, M. W. Mitchell, M. Markham, D. J. Twitchen, D. Elkouss, S. Wehner, T. H. Taminiau, and R. Hanson, Nature **526**, 682 (2015).
[9]J. R. Maze, P. L. Stanwix, J. S. Hodges, S. Hong, J. M. Taylor, P. Cappellaro, L. Jiang, M. V. G. Dutt, E. Togan, A. S. Zibrov, A. Yacoby, R. L. Walsworth, and M. D. Lukin, Nature **455**, 644 (2008).
[10]G. Balasubramanian, I. Y. Chan, R. Kolesov, M. Al-Hmoud, J. Tisler, C. Shin, C. Kim, A. Wojcik, P. R. Hemmer, A. Krueger, T. Hanke, A. Leitenstorfer, R. Bratschitsch, F. Jelezko, and J. Wrachtrup, Nature **455**, 648 (2008).
[11]L. Rondin, J.-P. Tetienne, T. Hingant, J.-F. Roch, P. Maletinsky, and V. Jacques, Rep. Prog. Phys. **77**, 056503 (2014).
[12]J. Wrachtrup, F. Jelezko, B. Grotz, and L. McGuinness, MRS Bull. **38**, 149 (2013).
[13]T. Schröder, S. L. Mouradian, J. Zheng, M. E. Trusheim, M. Walsh, E. H. Chen, L. Li, I. Bayn, and D. Englund, J. Opt. Soc. Am. B **33**, B65 (2016).
[14]K. Ohno, F. J. Heremans, L. C. Bassett, B. A. Myers, D. M. Toyli, A. C. Bleszynski Jayich, C. J. Palmstrøm, and D. D. Awschalom, Appl. Phys. Lett. **101**, 082413 (2012).
[15]K. Ohashi, T. Rosskopf, H. Watanabe, M. Loretz, Y. Tao, R. Hauert, S. Tomizawa, T. Ishikawa, J. Ishi-Hayase, S. Shikata, C. L. Degen, and K. M. Itoh, Nano Lett. **13**, 4733 (2013).
[16]K. Ohno, F. J. Heremans, C. F. de las Casas, B. A. Myers, B. J. Alemán, A. C. Bleszynski Jayich, and D. D. Awschalom, Appl. Phys. Lett. **105**, 052406 (2014).
[17]E. E. Kleinsasser, M. M. Stanfield, J. K. Q. Banks, Z. Zhu, W.-D. Li, V. M. Acosta, H. Watanabe, K. M. Itoh, and K.-M. C. Fu, Appl. Phys. Lett. **108**, 202401 (2016).
[18]J. Meijer, B. Burchard, M. Domhan, C. Wittmann, T. Gaebel, I. Popa, F. Jelezko, and J. Wrachtrup, Appl. Phys. Lett. **87**, 261909 (2005).

[19]J. R. Rabeau, P. Reichart, G. Tamanyan, D. N. Jamieson, S. Prawer, F. Jelezko, T. Gaebel, I. Popa, M. Domhan, and J. Wrachtrup, Appl. Phys. Lett. **88**, 023113 (2006).

[20]D. M. Toyli, C. D. Weis, G. D. Fuchs, T. Schenkel, and D. D. Awschalom, Nano Lett. **10**, 3168 (2010).

[21]P. Spinicelli, A. Dréau, L. Rondin, F. Silva, J. Achard, S. Xavier, S. Bansropun, T. Debuisschert, S. Pezzagna, and J. Meijer, New J. Phys. **13**, 025014 (2011).

[22]S. Pezzagna, D. Rogalla, H.-W. Becker, I. Jakobi, F. Dolde, B. Naydenov, J. Wrachtrup, F. Jelezko, C. Trautmann, and J. Meijer, Phys. Status Solidi A **208**, 2017 (2011).

[23]S. Sangtawesin, T. O. Brundage, Z. J. Atkins, and J. R. Petta, Appl. Phys. Lett. **105**, 063107 (2014).

[24]S. Pezzagna, B. Naydenov, F. Jelezko, J. Wrachtrup, and J. Meijer, New J. Phys. **12**, 065017 (2010).

[25]B. K. Ofori-Okai, S. Pezzagna, K. Chang, M. Loretz, R. Schirhagl, Y. Tao, B. A. Moores, K. Groot-Berning, J. Meijer, and C. L. Degen, Phys. Rev. B **86**, 081406 (2012).

[26]C. Osterkamp, J. Scharpf, S. Pezzagna, J. Meijer, T. Diemant, R. J. Behm, B. Naydenov, and F. Jelezko, Appl. Phys. Lett. **103**, 193118 (2013).

[27]D. Antonov, T. Häußermann, A. Aird, J. Roth, H.-R. Trebin, C. Müller, L. McGuinness, F. Jelezko, T. Yamamoto, J. Isoya, S. Pezzagna, J. Meijer, and J. Wrachtrup, Appl. Phys. Lett. **104**, 012105 (2014).

[28]S. M. Sze and M. K. Lee, *Semiconductor Devices: Physics and Technology*, 3rd ed. (Wiley, Hoboken, 2012).

[29]S. Cui, A. S. Greenspon, K. Ohno, B. A. Myers, A. C. Bleszynski Jayich, D. D. Awschalom, and E. L. Hu, Nano Lett. **15**, 2887 (2015).

[30]F. F. de Oliveira, S. A. Momenzadeh, Y. Wang, M. Konuma, M. Markham, A. M. Edmonds, A. Denisenko, and J. Wrachtrup, Appl. Phys. Lett. **107**, 073107 (2015).

[31]J. F. Zeigler, http://www.srim.org/ for The Stopping and Range of Ions in Matter, SRIM-2013.

[32]J. F. Zeigler, Nucl. Instrum. Methods Phys. Res. B **219-220**, 1027 (2004).

[33]K.-M. C. Fu, C. Santori, P. E. Barclay, and R. G. Beausoleil, Appl. Phys. Lett. **96**, 121907 (2010).

[34]A. Gali, M. Fyta, and E. Kaxiras, Phys. Rev. B **77**, 155206 (2008).

[35]N. Mizuochi, P. Neumann, F. Rempp, J. Beck, V. Jacques, P. Siyushev, K. Nakamura, D. J. Twitchen, H. Watanabe, S. Yamasaki, F. Jelezko, and J. Wrachtrup, Phys. Rev. B **80**, 041201 (2009).

[36]E. L. Hahn, Phys. Rev. **80**, 580 (1950).

[37]L. Childress, M. V. G. Dutt, J. M. Taylor, A. S. Zibrov, F. Jelezko, J. Wrachtrup, P. R. Hemmer, and M. D. Lukin, Science **314**, 281 (2006).

[38]L. M. Pham, S. J. DeVience, F. Casola, I. Lovchinsky, A. O. Sushkov, E. Bersin, J. Lee, E. Urbach, P. Cappellaro, H. Park, A. Yacoby, M. Lukin, and R. L. Walsworth, Phys. Rev. B **93**, 045425 (2016).

[39]M. Loretz, J. M. Boss, T. Rosskopf, H. J. Mamin, D. Rugar, and C. L. Degen, Phys. Rev. X **5**, 021009 (2015).

[40]F. F. de Oliveira, D. Antonov, Y. Wang, P. Neumann, S. A. Momenzadeh, T. Häußermann, A. Pasquarelli, A. Denisenko, and J. Wrachtrup, e-print arXiv:1701.07055v1.